Available online at www.sciencedirect.com
SCIENCE DIRECT®
Pergamon
Cement and Concrete Research 34 (2004) 165–174
CEMENT AND CONCRETE RESEARCH

Analyzing crack width to predict corrosion in reinforced concrete

T. Vidal, A. Castel, R. François*

Laboratoire Matériaux et Durabilité des Constructions (LMDC), Departement Genie Civil et Urbanisme, Institut National des Sciences Appliquees (INSA-UPS), 135 Avenue de Rangueil, 31077 Toulouse cedex 4, France

Received 15 March 2002; accepted 22 July 2003

Abstract

Our aim in this paper is to introduce a set of relationships linking the distribution of reinforcement corrosion and the width of cover crack that results from such corrosion. This work is based on experimental results obtained on the longitudinal reinforcements of two beams naturally corroded over periods of 14 and 17 years. We first compared these experimental results with existing models linking crack width and attack penetration. Noting that such models only partially predict actual experimental data, we put forward a new model using the parameter of reinforcement cross-section loss.

Keywords: Corrosion; Reinforcement; Concrete; Crack detection; Modeling

1. Introduction

Since 1984, Laboratoire Matériaux et Durabilité des Constructions (LMDC) in Toulouse has been conducting a major research project to gain a better understanding of the relationship between mechanical loading and the development of reinforcement corrosion in reinforced concrete structures exposed to an aggressive environment. A model for corroded reinforced concrete behavior was recently proposed [1], taking into account the combined effects of corrosion as shown in a reduction in bar section and to loss of the steel–concrete bond [2–7]. Reinforcement cross-section loss is the main input parameter for this model, allowing us to predict mechanical behavior of the corroded reinforced concrete. To this purpose, in situ evaluation of the corrosion state of the corroded structures was essential.

As we proceed with in situ testing, we are aware that there are some nondestructive methods, as with the linear polarization technique [8,9], available that can provide data on the corrosion rate of the reinforcements embedded in concrete. But without precise information on changes in the rate of corrosion over time, these methods cannot provide us with the means to evaluate actual cross-section reduction. Another technique, with RADAR measurements [10], only detects whether conditions are propitious to growth in corrosion through analysis of the concrete's electromagnetic properties.

The purpose of the study is to assess the state of corrosion of in situ corroded structural elements by visual inspection, and to establish the local distribution of corrosion on each reinforcement.

Thus, one approach involves deducing the reduction in the steel cross-section from observing the width of cracks due to corrosion. Indeed, longitudinal cracks provide the clearest visual manifestation of reinforcement corrosion. This phenomenon arises from the formation of corrosion products, which are more voluminous than sound steel. Radial stresses generated on the surrounding concrete make the concrete cover crack.

Some experimental works [11,12] attempt to link longitudinal crack width with corrosion but, as a general rule, they rely on accelerated tests using electrical fields that provide a poor substitute for real corrosion. Conversely, our experimental results in the present study were obtained from two beams naturally corroded in a saline environment and subjected to wetting–drying cycles over periods of 14 and 17 years. Although this represents an accelerated version of the real process, the corrosion

* Corresponding author. Tel.: +33-5-61-55-99-05; fax: +33-5-61-55-99-00.
E-mail address: raoul.francois@insa-tlse.fr (R. François).

0008-8846/$ – see front matter © 2003 Elsevier Ltd. All rights reserved.
doi:10.1016/S0008-8846(03)00246-1

obtained was much closer to that actually observed in natural conditions, with respect to corrosion distribution, corrosion type and the oxides produced, than that resulting from use of an impressed current or a $CaCl_2$ admixture in concrete.

Our reduced sample population can be explained by the long duration needed to ensure propagation of corrosion. However, four 3-m-long reinforcements were embedded in each beam, with various covercrete and bar diameter values. To all practical purposes, we could therefore consider every reinforcement area (each including one pit of corrosion ~ 0.5 mm long) as providing an individual sample. Thus, considering the impressive expansion due to corrosion, the number of samples for each reinforcement turns out to be quite significant.

Our first step was to compare the results obtained with existing models linking crack width and corrosion. We then introduced new relationships between local distribution of steel cross-section loss and corresponding longitudinal crack width, taking into account the influence of different parameters such as cover/diameter ratio and bar diameter.

2. Experimental context

This work was based on a long-term experimental program started in 1984 at LMDC [13]. Initially, 36 reinforced concrete beams were cast and stored under loading in a chloride environment. At different stages, beams were extracted from the chloride environment to carry out experimental works to assess chloride penetration, consider the effect of cracks on corrosion, etc. We provided a summary of the first 12 years of experiments in a previous paper [14]. At present, 12 beams are still stored under loading in confined salt fog and we are now studying the results obtained on two individuals extracted from this set of beams. The salient feature of this sustained experiment is that corrosion results from storage in a chloride environment in a loading state, the "natural" corrosion thus obtained being highly representative of corroded structures out in the real world. The chloride environment (35 g/l of NaCl, corresponding to the salt concentration of sea water) is generated through the use of four sprays located in each upper corner of a confined room, with wetting–drying cycles.

Reinforced concrete members are 3-m-long beams (150 × 280 mm cross section). Type A and B beams have different reinforcements but use the same ordinary reinforcing steel (yield strength = 500 MPa). Beams A and B correspond to a 40-mm maximum and 10-mm minimum concrete cover, respectively (Fig. 1), in accordance with French regulations at the time of manufacturing (BAEL 1983). According to French standards, the loading value (M_{ser} = 13.5 kN · m) corresponded to maximum loading versus durability in an aggressive environment for the type A beam (serviceability limit state requirements in an aggressive environment) and to maximum loading versus resistance (ultimate load limit state in a nonaggressive environment) for the type B element. In cracked sections, the maximum stresses in the tensile reinforcements were 165 and 250 MPa, respectively, for samples A and B. Despite creeping, loading rates were kept constant using an appropriate device.

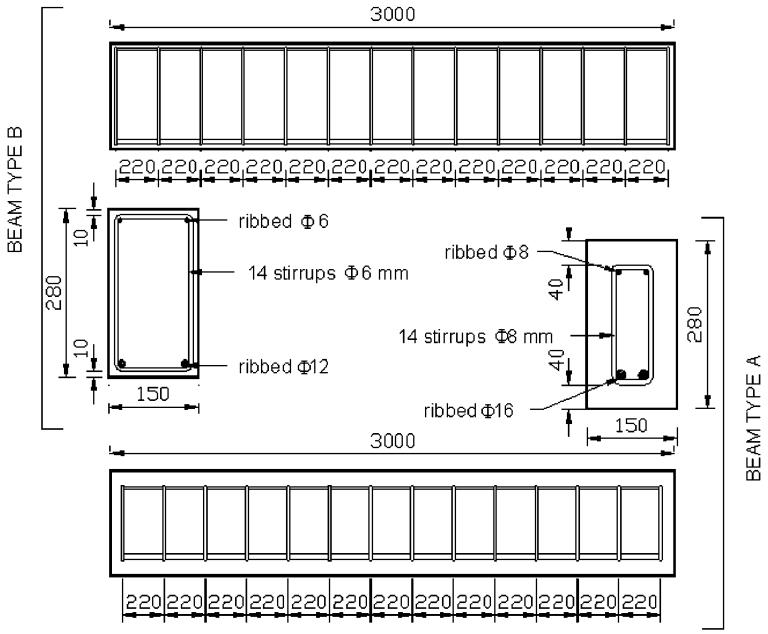

Fig. 1. Lay-out of the reinforcement (all dimensions in mm) for types A and B beams.

Table 1
Concrete composition

Mix component	(mm)	(kg/m^3)
Rolled gravel (Silica + Limestone)	5/15	1220
Sand	0/5	820
Portland Cement: OPC HP (high performance)		400
Water		200

Cement composition

	SiO_2	Al_2O_3	Fe_2O_3	CaO	MgO	SO_3	Na_2O
% weight	21.4	6.0	2.3	63.0	1.4	3.0	0.5

Concrete composition and cement chemical composition are given in Table 1. The water/cement ratio was 0.5 but the water content was adjusted (i.e. 0.49 or 0.48) to obtain a constant workability of 7 cm in slump test. The average compression stress and the elastic modulus obtained on cylinder specimens were, respectively, 45 MPa and 32 GPa at 28 days. The tensile strength, measured using the splitting test, was 4.7 MPa. Porosity was 15.2%.

3. Experimental program

The research work was based on experimental results obtained on A and B elements taken out after 17 and 14 years of storage in a saline environment.

3.1. Cracking maps

For each beam, cracking maps were specifically drawn with the exact locations of flexural transverse cracks and longitudinal corrosion cracking. A binocular lens with an accuracy of 0.02 mm was used to measure cracks widths. As we only link the steel cross-section loss with the width of corrosion cracks, the widths of flexural cracks are not indicated on the cracking maps.

3.2. Assessment of the reinforcement cross-section loss

We evaluated the steel cross-section loss from the reinforcement loss of mass. Reference mass of reinforcement per unit of length was measured using bars in non corroded areas. In corroded areas, the residual mass per unit of length was evaluated after removal of corrosion products (using a Clark's solution) and then related to the reference mass. The average reinforcement loss of mass per unit of length was then calculated using Eq. (1):

$$\Delta m = m - m' \tag{1}$$

with Δm: mass loss per unit of length; m': residual mass per unit of length; m: reference mass per unit of length.

The measure of corrosion damage was performed on all the reinforcements of each beam. The steel cross-section loss was finally deduced from loss of mass using Eq. (2):

$$\Delta A_s = \frac{\Delta m}{m} A_s \tag{2}$$

with ΔA_s: steel cross-section loss (mm^2); A_s: sound steel cross-section (mm^2).

4. Comparison method between experimental results and existing models

Most research work [11,12] dealing with the relationships between corrosion and crack width are based on the attack penetration parameter. Thus, in a first step, results are transposed in terms of the attack penetration parameter and compared with existing research works carried out at the Institute Eduardo Torroja and at Geocisa in Madrid [11,12].

4.1. Determination of attack penetration

Attack penetration (Fig. 2) was calculated from measured steel loss of mass using the Rodriguez et al. [11] method. Eq. (3) gives the relation between pit attack and reinforcement diameter decrease [11]:

$$\phi = \phi_0 - \alpha x \tag{3}$$

where ϕ is the residual bar diameter; ϕ_0 is the initial bar diameter; x is the pit penetration; α is the pit concentration factor [15]; $\alpha = 2$, for homogeneous corrosion; $4 < \alpha < 8$, for localized corrosion.

We then obtained the relation between corrosion pit depth and steel cross-section loss by coupling Eqs. (1)–(3):

$$x = \frac{\phi_0}{\alpha}\left[1 - \sqrt{1 - \frac{\Delta A_s}{A_s}}\right] 10^3 \tag{4}$$

where x is the pit penetration (μm); ϕ_0 is the initial bar diameter (mm).

We deduced the values of the pit depths from the measured local reinforcement cross-section loss thanks to Eq. (4). The pit concentration factor was equal to 8,

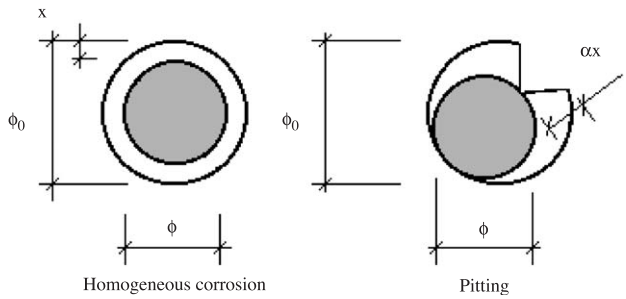

Fig. 2. Residual reinforcing bar section (from Rodriguez et al. [11]).

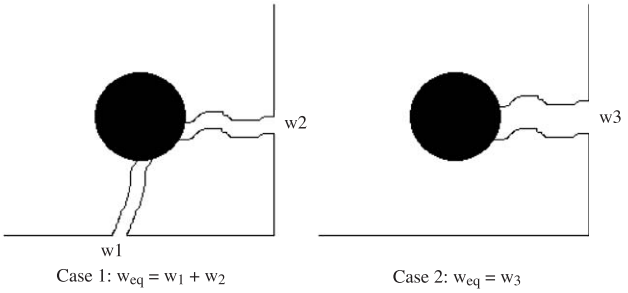

Fig. 3. Example of two equivalent crack configurations for a same corrosion state.

corresponding to the value for a localized corrosion attack induced by chlorides.

4.2. Determination of the crack width corresponding to attack penetration

For one location of the beam, the sum of crack widths on the two beam surfaces, due to the same corroded area of one bar, was calculated. An example is shown in Fig. 3, considering two crack configurations. For configuration 1, the equivalent width w_{eq} corresponds to the sum of the width of both cracks. For configuration 2, the equivalent width w_{eq} corresponds to the width of crack w_3.

5. Experimental results

5.1. Cracking maps

Cracking maps were drawn with the widths of the longitudinal corrosion cracks (Figs. 4 and 5). The transversal straight lines correspond to the flexural cracks induced by the mechanical loading. However, their widths are not indicated because they are not generated by corrosion. Then, beams were broken in order to assess local reinforcement corrosion.

5.2. Distribution of reinforcement cross-section loss

Corrosion distribution assessment was performed on tensile bars and on bars in concrete compressive zones for both beams. The local reinforcement cross-section loss was calculated from the local loss of mass using Eq. (2) (Figs. 6–9).

6. Relationships between crack width and attack penetration

Attack penetrations resulting from local losses of mass were related to the crack width measured on both beams in Fig. 10. Four types of bars were studied: bars in the concrete compressive zone and tensile bars of beams A and B.

Comparison between experimental results and existing models was conducted through both steps of the cracking process:

–initiation;
–propagation.

6.1. Attack penetration initiating cracking

The graphs depicting crack width versus attack penetration, based on the experimental results, are used to determine the experimental attack penetration x_0, initiating cracking on type A and B beams (Fig. 10). The abscissa of the intersection point between the linear trend

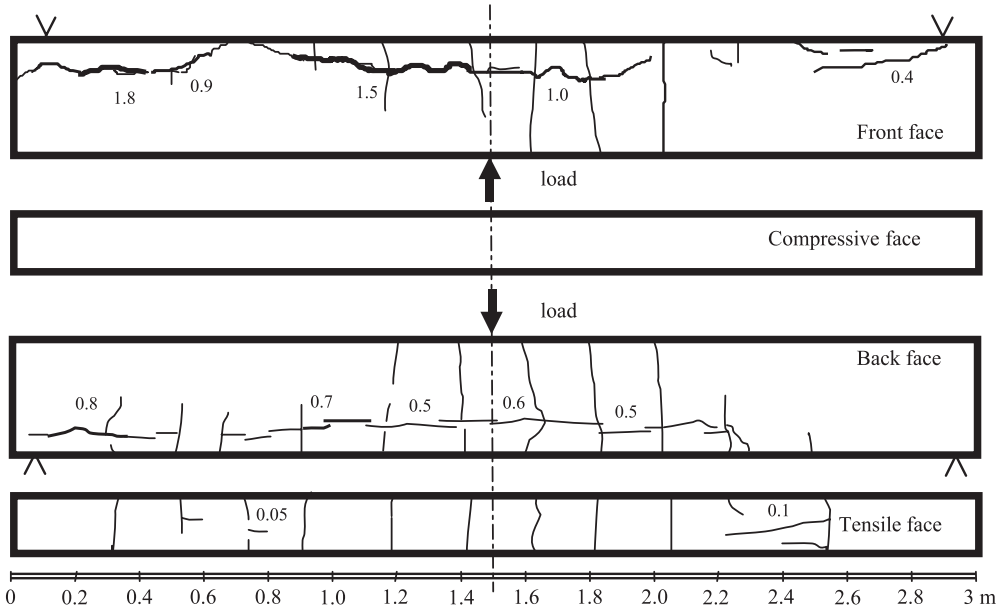

Fig. 4. Cracking map of beam A (all crack widths are in millimeters).

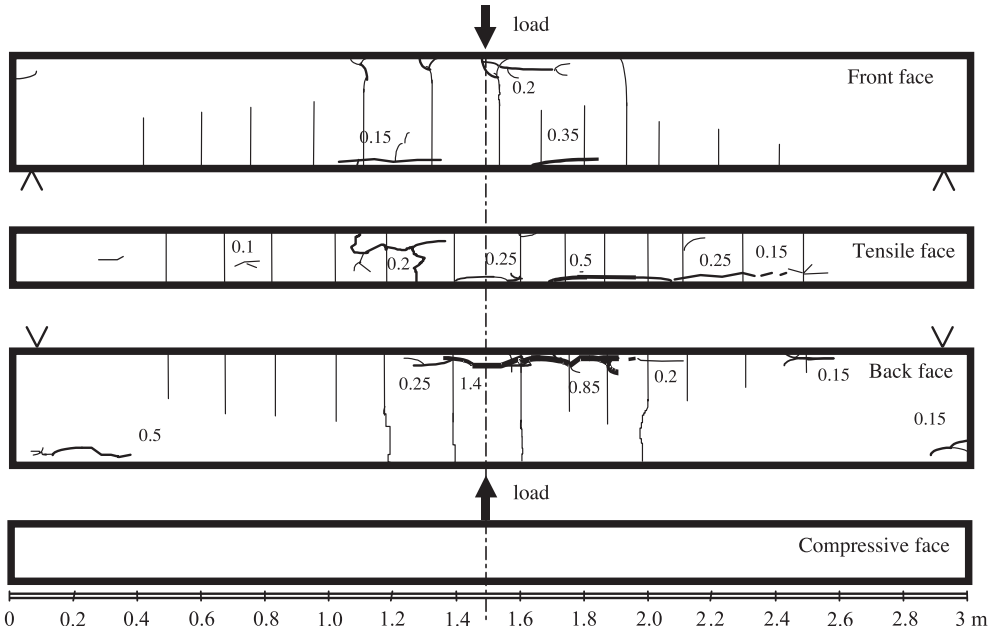

Fig. 5. Cracking map of beam B (all crack widths are in millimeters).

curve of experimental points and the abscissa axis corresponds to the attack penetration required to crack covercrete.

Only three values of attack penetration x_0 inducing cracks are therefore obtained since no cracks appeared in the case of bars in the concrete compressive zone of beam A. In accordance with the results from other studies [11,12,16], the most significant parameter influencing cracking initiation was the cover/diameter ratio (Fig. 11). As concrete cover corresponds to the thickness of concrete between transverse reinforcement (stirrups) and concrete surface, the concrete thickness between longitudinal reinforcement and beam surface is 4.8 and 1.6 cm, respectively, for beams A and B. These values are used to calculate the c/ϕ_0 ratio, with ϕ_0 corresponding to the initial diameter of the longitudinal reinforcement.

In Fig. 11, experimental results are compared with existing models Eq. (5) [12] and Eq. (6) [11]. These linear relationships link attack penetration required to initiate cracking x_0 and the cover/diameter ratio:

$$x_0 = 7.53 + 9.32\frac{c}{\phi_0} \quad (5)$$

[12] where x_0 is the pit penetration needed for cracking initiation (μm); c is the concrete cover (mm); ϕ_0 is the initial bar diameter (mm).

$$x_0 = 83.8 + 7.4\frac{c}{\phi_0} - 22.6 f_{c,sp} \quad (6)$$

[11] where $f_{c,sp}$ is the splitting tensile strength (MPa).

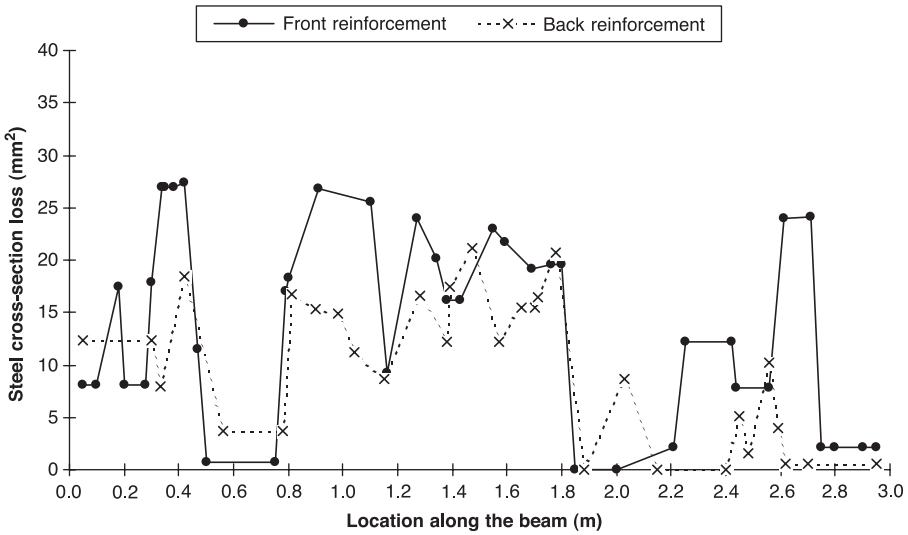

Fig. 6. Distribution of corrosion along beam A for reinforcements in concrete tensile zone.

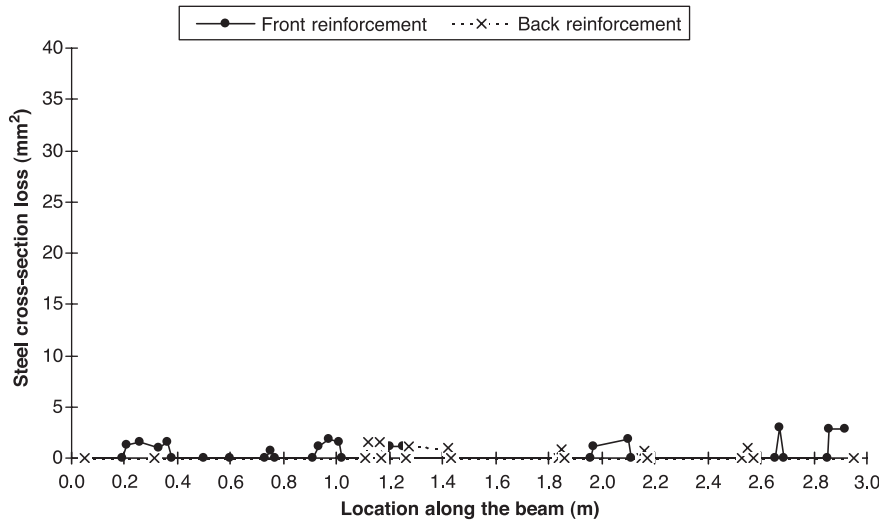

Fig. 7. Distribution of corrosion along beam A for reinforcements in concrete compressive zone.

The main difference between Eqs. (5) and (6) is the influence of concrete tensile strength on x_0, which is taken into account in Eq. (6). However, Fig. 11 shows that the experimental results were not compliant with the predictions calculated using Eq. (6). Indeed, for the beams used in the study and for a concrete tensile strength equal to 4.7 MPa, model predictions become erroneous ($x_0 < 0$). Conversely, Eq. (5) seems to be relevant. Considering the good correlation obtained, Eq. (5) will be used to predict x_0 in the remainder of the study.

6.2. Relation between crack width and attack penetration

As previously indicated, the corrosion of bars in concrete compressive zones for beam A did not generate any crack. For this case, only the maximum pit penetration is indicated. Fig. 10 shows the development of crack width versus attack penetration, including experimental results and existing models.

The general form of the relationship between crack width and attack penetration proposed by Rodriguez et al. [11] is:

$$w = K(x - x_0) \tag{7}$$

where w is the crack width (mm); K is the slope of the curve; x_0 is the attack penetration causing crack initiation (μm).

In 1996, Rodriguez et al. [11] proposed the following expression:

$$w = 0.05 + \beta(x - x_0) \tag{8}$$

where β is a coefficient depending on the bar position ($\beta = 0.01$ for top cast bars and 0.0125 for bottom cast bars).

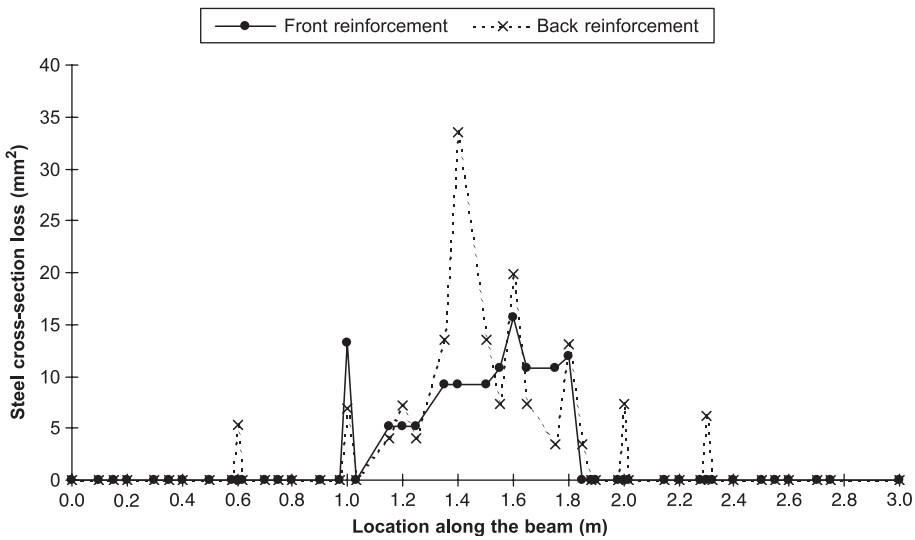

Fig. 8. Distribution of corrosion along beam B for reinforcements in concrete tensile zone.

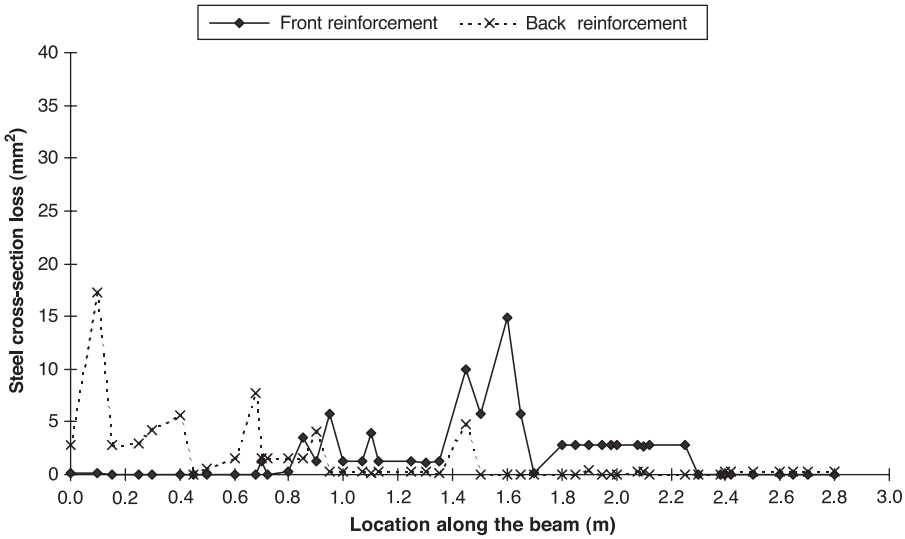

Fig. 9. Distribution of corrosion along beam B for reinforcements in concrete compressive zone.

In Fig. 10, the modeled curves were calculated using Eq. (8). The pit attack initiating cracking, x_0 is calculated with Eq. (5).

Analysis of Fig. 10 suggests that these methods are not really suited to experimental results. Moreover, the value of parameter α ($\alpha = 8$) corresponds to the best correlation between the Rodriguez et al. model and experimental results (see paragraph 4). In the cases of the tensile reinforcements of beam A and that for the reinforcements located in the compressive zone of beam B, correlation between the opening of the corrosion cracking and attack penetration is different, in spite of a similar cover/diameter ratio. In accordance with analysis by Rodriguez et al., the cover/diameter ratio seems not to be correlated with the

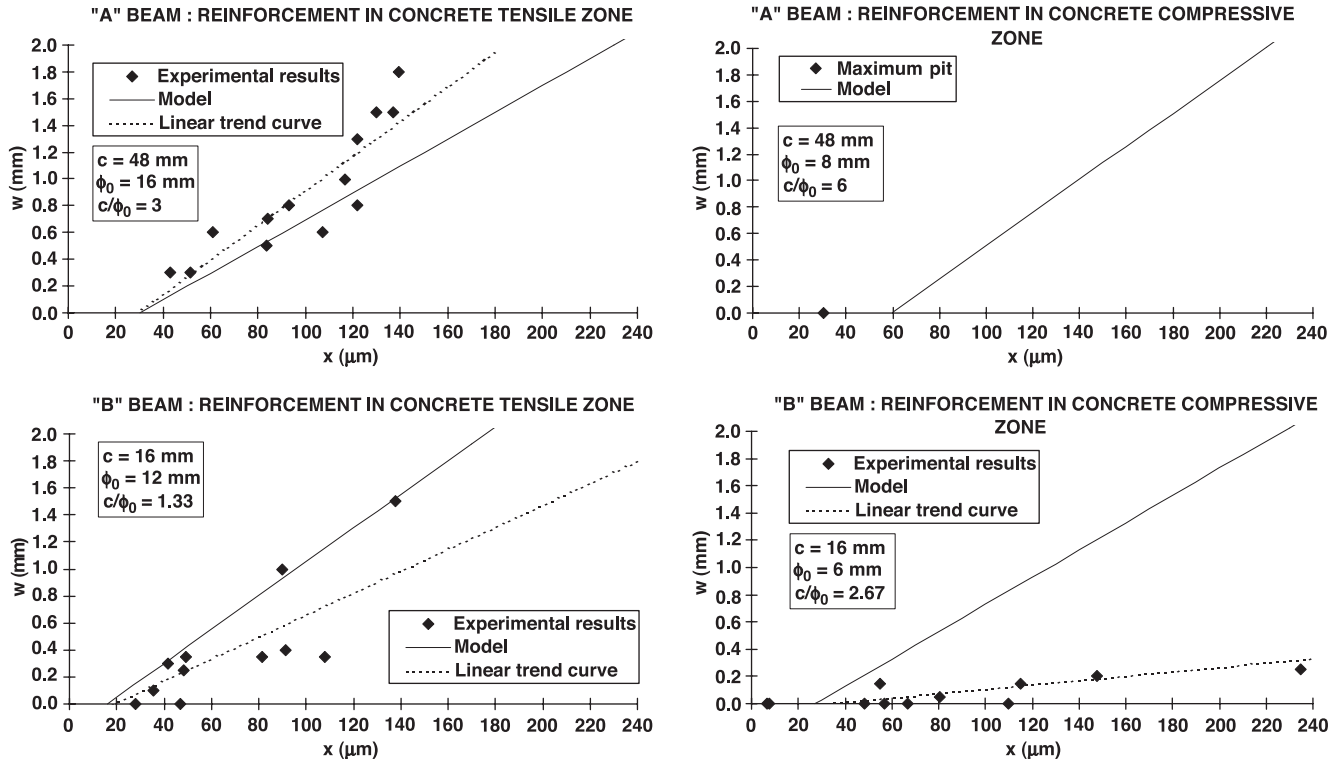

Fig. 10. Crack width evolution versus attack penetration for longitudinal reinforcements of beams A and B, and for different values of concrete cover, diameter and c/ϕ_0 ratio.

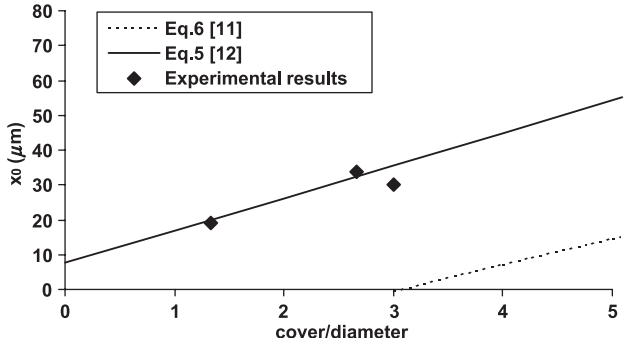

Fig. 11. Relation between attack penetration which generates cracking initiation and cover/diameter ratio.

development of cracking. This difference between the two cases could be explained by the fact that these reinforcements have a different diameter. The diameter, which is not taken into account, would then seem to have some influence on the relationship between crack width and attack penetration.

During the propagation process, the crack width is directly linked to the volume of oxides, which is proportional to the steel cross-section loss. A linear relationship linking the reinforcement cross-section loss and the crack width could be proposed. Thus, this relation will be independent of the reinforcement diameter.

According to other authors [11], the relationship (Eq. (8)) between pit depth and crack width would be also independent of the reinforcement diameter. However, considering the configurations of two different diameter reinforcements with the same attack penetration (as shown in Fig. 12), the reinforcement cross-section loss given in Eq. (9), from Eq. (3), is obviously dependent on the bar diameter ϕ_0:

$$\Delta A_s = \frac{\pi}{4}(2\alpha x\phi_0 - \alpha^2 x^2) \tag{9}$$

Thus, two similar pit depths occurring on two different diameters induce varying steel cross-section losses and crack widths. This explains the differences between our experimental results and the models (Fig. 10).

In conclusion, existing models could only partially predict our experimental results based on real corrosion conditions.

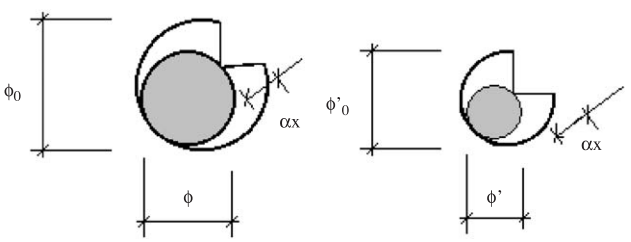

Fig. 12. Example of two configurations of loss of steel section induced by the same attack penetration (αx) on two different diameter reinforcements (from Rodriguez et al. [11]).

We shall therefore propose a new relationship between the crack width and the reinforcement cross-section loss.

7. A new model linking crack widths and reinforcement cross-section losses

The cross-section loss parameter is chosen to describe the cracking process rather than pit penetration. The new model predicting reinforcement cross-section loss from crack width is exposed through the two phases: initiation and propagation.

7.1. Steel cross-section loss initiating cracking

In the light of the comments made on Fig. 10, we choose the model proposed by Alonso et al. (Eq. (5)) to predict the steel cross-section loss ΔA_{s0} initiating cracks. We can then combine Eqs. (4) and (5) to obtain the expression of the local steel cross-section loss ΔA_{s0} necessary for cracking initiation versus ϕ_0, A_s, α and the c/ϕ_0 ratio (Eq. (10)):

$$\Delta A_{s0} = A_s\left[1 - \left[1 - \frac{\alpha}{\phi_0}\left(7.53 + 9.32\frac{c}{\phi_0}\right)10^{-3}\right]^2\right] \tag{10}$$

where ϕ_0 is the bar diameter (mm); α is the pit concentration factor [13]; c is the covercrete (mm); ΔA_{s0} is the steel cross-section loss (mm^2); A_s is the sound steel cross section (mm^2).

Eq. (10) does not take the concrete characteristics (concrete tensile strength, porosity, etc.) into account [12] because the beams used for this study were cast using the same concrete. Thus, the experimental data available allow for no conclusions to be drawn on the influence of concrete characteristics. In Table 2, experimental and calculated steel cross-section losses are practically identical. Experimental steel cross-section loss values are determined, using Eq. (9), from the pit attack corresponding to the abscissa of the point of intersection between the linear trend curve of experimental points and the abscissa axis (Fig. 10).

7.2. Relation between crack widths and steel cross-section loss

Fig. 13 illustrates the crack width measured on the concrete beam in relation to the steel cross-section loss. For each case of reinforcement, the value of the steel

Table 2
Comparison between experimental and calculated value of steel cross-section loss initiating cracking

Beam	Reinforcement	Experimental value (mm^2)	Calculated value (mm^2)
A	concrete tensile zone	6.08	7.07
	concrete compressive zone	maximum: 3.01	6.18
B	concrete tensile zone	2.90	2.99
	concrete compressive zone	2.49	2.39

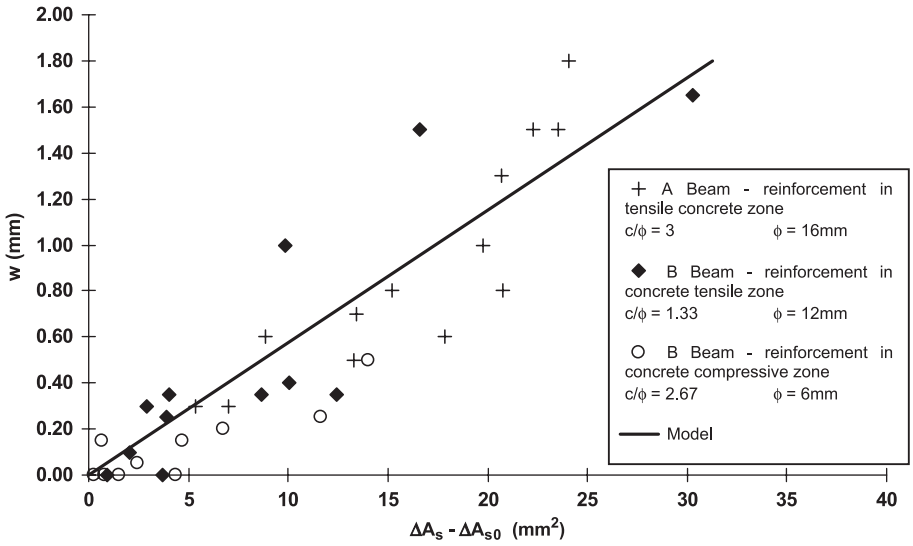

Fig. 13. Crack width evolution versus steel loss of section for reinforcements of beams A and B.

cross-section loss initiating cracking is deduced from experimental points in order to represent only the propagation step of the cracking process. As the maximum cross-section loss did not generate cover cracking, the experimental results of the reinforcement in concrete compressive zone of beam A are not shown in Fig. 13. The empirical linear expression predicting crack propagation is as follows:

$$w = K(\Delta A_s - \Delta A_{s0}) \quad (11)$$

where w is the crack width (mm); ΔA_s is the steel loss of cross-section in mm^2; $K = 0.0575$; $r^2 = 0.82$ (from the regression).

Fig. 13 shows that experimental values are correctly correlated using a single linear relationship, independent of the c/ϕ_0 and diameter parameters. This confirms and justifies the use of the reinforcement cross-section loss, instead of attack penetration, as the single parameter influencing the growth of cracks in the propagation phase, for present results.

However, the position of the bar taken into account by the Rodriguez et al. model (coefficient β) seems to have no influence on cracking development. Indeed, it is well known [17–19] that the quality of the steel–concrete interface will vary, in relation to steel localization in the beam, because local steel concrete debonding due to concrete bleeding occurs under the upper bar with respect to the casting direction. If there are more voids around upper bars, corrosion products will have to fill in this local porosity before cracking; thus, only the value of pit initiating cracking will be affected. Crack appearance will be delayed [7], but after initiation, the steel position has no influence.

Nevertheless, Fig. 13 shows relatively significant scatter. For crack width values ranging between 0 and 1 mm, scatter seems less significant than for values ranging over 1 mm. This concurs with the results from Alonso et al. [12].

8. Conclusions

In this research work, we studied the crack widths and reinforcement losses of mass due to corrosion of two 3-m-long reinforced concrete beams stored in a chloride environment. Corrosion of reinforcements was close to such corrosion as occurs in natural conditions with respect to distribution, corrosion type and types of oxides produced. The significant amount of corrosion and the wide distribution of attack penetrations along the reinforcements produced an extensive set of experimental points linking crack width to corrosion.

In the first instance, the corrosion state is expressed in terms of attack penetration thanks to the formula provided by Rodriguez et al. and then compared with existing models of crack width development versus corrosion pitting. However, while these models provide good predictions for crack initiation they have little to tell us about the propagation stage.

Thus, a new model linking crack width development to steel cross-section loss is proposed. Further, the steel cross-section loss is a better input parameter for mechanical models of corroded reinforced concrete behavior.

The two steps of the cracking process, crack initiation and propagation have been analyzed with respect to different factors such as the cover/diameter ratio and the bar diameter.

1. Crack initiation: depends on the c/ϕ_0 ratio and the bar diameter, but the quality of the steel concrete interface may have some effect.

2. Crack propagation: the cover/diameter ratio and the bar diameter seem to have no effect on the crack width evolution as a function of steel cross-section loss.

In conclusion, the local state of corroded reinforcements can be assessed thanks to an empirical relationship between the crack width and the steel cross-section loss, which seem to be independent of the bar diameter, and the cover/diameter ratio— except when it comes to crack initiation. However, more experimental data should allow us to refine our knowledge of these relationships by testing beams with various reinforcement diameters, cover, porosity (or water/cement ratio, which is directly linked) and tensile concrete strength.

References

[1] A. Castel, R. François, G. Arliguie, Mechanical behavior model of corroded reinforced concrete, C. R. Acad. Sci. Mech. 330 (2002) 45–50.
[2] J.A. Gonzalez, S. Feliù, P. Rodriguez, E. Ramirez, C. Alonso, C. Andrade, Some questions on the corrosion of steel in concrete: Part I. When, how, and how much steel corrodes, Mater. Struct. 29 (1996) 40–46.
[3] P.S. Mangat, M.S. Elgarf, Bond characteristics of corroding reinforcement in concrete beams, Mater. Struct. 32 (1999) 89–97.
[4] G.J. Al-Sulaimani, M. Kaleemullah, I.A. Basunbul, Rasheeduzzafar, Influence of corrosion and cracking on bond behavior and strength of reinforced concrete members, ACI Struct. J. 87 (2) (1990) 220–231.
[5] A.A. Almusallam, A.S. Al-Gahtani, A.R. Aziz, Rasheeduzzafar, Effect of reinforcement corrosion on bond strength, Constr. Build. Mater. 10 (2) (1996) 123–129.
[6] A. Castel, R. François, G. Arliguie, Mechanical behavior of corroded reinforced concrete beams: Part 1. Experimental study of corroded beams, Mater. Struct. 33 (2000) 539–544.
[7] A. Castel, R. François, G. Arliguie, Mechanical behavior of corroded reinforced concrete beams: Part 2. Bond and notch effects, Mater. Struct. 33 (2000) 545–551.
[8] S. Feliu, J.A. Gonzalez, S. Feliu Jr., C. Andrade, Confinement of the electrical signal for in situ measurement of polarization resistance in reinforced concrete, ACI Mater. J., (1990) 457–460.
[9] J. Rodriguez, L.M. Ortega, A.M. Garcia, L. Johansson, K. Petterson, On-site corrosion measurements in concrete structures, Constr. Repair, (1995) 27–30.
[10] J. Rhazi, S. Laurens, G. Ballivy, Insights on the GPR non destructive testing method of bridge decks, Special Session on Non Destructive Detection of Corrosion in Reinforced Concrete, ACI Meeting, Toronto, 2000.
[11] J. Rodriguez, L.M. Ortega, J. Casal, J.M. Diez, Corrosion of reinforcement and service life of concrete structures, Durab. Build. Mater. Compon. 7 (1) (1996) 117–126.
[12] C. Alonso, C. Andrade, J. Rodriguez, J.M. Diez, Factors controlling cracking of concrete affected by reinforcement corrosion, Mater. Struct. 31 (1998) 435–441.
[13] R. François, G. Arliguie, J.C. Maso, Durability of Reinforced Concrete, Internal Synthesis Report L.M.D.C. I.N.S.A.-U.P.S. Toulouse, France (1994) (in French).
[14] R. François, G. Arliguie, Effect of microcracking and cracking on the development of corrosion in reinforced concrete members, Mag. Concr. Res. 51 (2) (1999) 143–150.
[15] J.A. Gonzalez, C. Andrade, C. Alonso, S. Feliù, Comparison of rates of general corrosion and maximum pitting generation on concrete embedded steel reinforcement, Cem. Concr. Res. 25 (2) (1995) 257–264.
[16] A.A. Torres-Acosta, A.A. Sagues, Concrete cover cracking with localized corrosion of reinforcing steel, in: V.M. Malhotra (Ed.), Fifth CANMET/ACI International Conference on Durability of Concrete, vol. 1, ACI, SP192, Barcelona, Spain, 2000, pp. 591–611.
[17] A. Castel, R. François, G. Arliguie, Factors other than chloride level influencing corrosion rate of reinforcement, in: V.M. Malhotra (Ed.), Fifth CANMET/ACI International Conference on Durability of Concrete, vol. 1, ACI, SP192, Barcelona, Spain, 2000, pp. 629–644.
[18] T. Yonezawa, V. Ashworth, R.P.M. Procter, Pore solution composition and chloride effects on the corrosion of steel in concrete, Corros. Eng. 44 (7) (1988) 489–499.
[19] T.U. Mohammed, N. Otsuki, M. Hisada, Corrosion of steel bars with respect to orientation in concrete, ACI Mater. J. (1999) 154–159.